Int. J. Heat Mass Transfer. Vol. 37, No. 1, pp. 153–164, 1994
Printed in Great Britain

0017–9310/94 $6.00 + 0.00

Analysis of two-dimensional hyperbolic heat conduction problems

HAN-TAW CHEN and JAE-YUH LIN
Department of Mechanical Engineering, National Cheng Kung University, Tainan, Taiwan 701, R.O.C.

(*Received* 24 *April* 1993)

Abstract—Two-dimensional hyperbolic heat conduction problems are investigated by using the hybrid numerical scheme. The thermal wave of such problems propagates with a finite velocity. Thus numerical oscillations in the vicinity of the thermal wave front can be observed, and a hybrid numerical method is presented, to reduce these oscillatory magnitudes. This method is that the time-dependent terms in the governing differential equations are removed by using the Laplace transform technique, and then the control volume method is used to discretize the space domain in the transform domain. The key of the present method is the selection of the shape functions. Various examples with the irregular geometry are illustrated.

INTRODUCTION

WITH THE advent of science and technology involving very low temperatures near absolute zero, extremely short transient duration and very high heat fluxes, some investigators found that the heat propagation velocity of such problems becomes finite. Peshkov [1] experimentally determined the velocity of thermal wave in helium II to be 19 m s^{-1} at a temperature of 1.4 K. Human [2] found that the thermal propagation becomes dominant for short-pulse laser heating. Maurer and Thompson [3] also found that if the surface heat fluxes are greater than the order 10^7 W cm^{-2}, the Fourier heat flux model will fail. To account for the phenomena involving the finite propagation velocity of the thermal wave, the classical Fourier heat flux model should be modified. Cattaneo [4] and Vernotte [5] suggested independently a modified heat flux model in the form of

$$\tau\frac{\partial q}{\partial t}+q=-k\nabla T \tag{1}$$

where q is the heat flux vector, k is the thermal conductivity and τ is the relaxation time. Sieniutycz [6] quoted that the τ values for homogeneous substance are of the order 10^{-8} to 10^{-12} s. However, for nonhomogeneous materials, Luikov [7] found that the τ values are of the order 10^{-3} to 10^{3} s. Recently, Kaminski [8] determined experimentally that the τ values for nonhomogeneous inner structure materials, such as glass ballotini, sand, H acid, etc., ranges from 10 s (for glass ballotini) to 50 s (for ion exchanger). The equation of energy conservation for such problems is given as

$$\rho C_p\frac{\partial T}{\partial t}=-\nabla\cdot q \tag{2}$$

where ρ is the density and C_p is the specific heat.

Elimination of q between equations (1) and (2) leads to the hyperbolic heat conduction equation.

$$\tau\frac{\partial}{\partial t}\left(\rho C_p\frac{\partial T}{\partial t}\right)+\rho C_p\frac{\partial T}{\partial t}=\nabla\cdot(k\nabla T). \tag{3}$$

Various analytical and numerical methods [3, 9–13] have been proposed to solve hyperbolic heat conduction problems. However, most methods are restricted to the analysis of one-dimensional problems. Due to the complicated reflection and interaction of thermal waves, multi-dimensional hyperbolic heat conduction problems are much more difficult to solve than one-dimensional problems. To the best of the authors' knowledge, only Yang [14] applied high-resolution numerical schemes to solve two-dimensional hyperbolic heat conduction problems. Yang [14] formulated the hyperbolic heat conduction (HHC) equations in an arbitrary body-fitted coordinate grid. The high-order non-oscillatory numerical schemes applied to one-dimensional HHC equation [13] was extended to two-dimensional problems by using the fractional step method. All calculations in the work of Yang [14] were performed using Roe's superbee limiter [13]. At the same time, the finer grid size and $\nu = 0.4$ are also required, where ν denotes the Courant–Friedrichs–Lewy (CFL) number. It can be seen that the work of Yang [14] did not show the actual numerical values of the investigated problems. Thus the comparative task between the present results and his results [14] is not made. The purpose of the present study is to provide a simpler approach to solve two-dimensional HHC problems without severe numerical oscillations.

The authors have developed an efficient numerical scheme involving the Laplace transform technique and the control volume method for one-dimensional HHC problems [15], and excellent comparisons with analytical results were obtained for various cases. The

NOMENCLATURE

C_p	specific heat
c	propagation velocity of thermal wave
i	unit vector in the x-direction
j	unit vector in the y-direction
k	thermal conductivity
N	shape function
Q	dimensionless heat flux
$\tilde{Q}$	Laplace transformed dimensionless heat flux
q	heat flux
s	Laplace transform parameter
T	temperature
T_0	ambient temperature
T_{in}	initial temperature
t	time
x	space coordinate in x-direction
y	space coordinate in y-direction.

Greek symbols

α	thermal diffusivity, $k/\rho C_p$
ζ	dimensionless space coordinate in y-direction
η	dimensionless space coordinate in x-direction
θ	dimensionless temperature
$\tilde{\theta}$	Laplace transformed dimensionless temperature
λ	coefficient in governing differential equation
ν	Courant–Friedrichs–Lewy number
ξ	dimensionless time
ρ	density
τ	relaxation time
Ω	control volume.

present study extends this numerical scheme to two-dimensional problems, with Laplace transform method used to remove the time-derivative terms from the governing equation, and then, the discretized expression of the transformed governing equation is derived by using the control volume method. The authors' previous work [15] has proved that the selection of the shape function is an important task for accurately predicting the propagation of the thermal wave, and the hyperbolic shape function for one-dimensional problems has been derived from the associated homogeneous differential equation in the transform domain to suppress successfully the numerical oscillations [15]. Thus a bi-hyperbolic shape function for two-dimensional problems is obtained by using the similar technique, and the numerical inversion of the Laplace transform is used to invert the transformed temperature to the physical result. It is found that the numerical instability induced by the bad choice of ν will not be found in the present study. Hence, the present method can suppress the numerical oscillations.

MATHEMATICAL FORMULATION

It is seen from equation (3) that a two-dimensional hyperbolic heat conduction equation with constant thermal properties in a rectangular coordinate system can be written as

$$\tau\rho C_p\frac{\partial^2 T}{\partial t^2}+\rho C_p\frac{\partial T}{\partial t}=k\left(\frac{\partial^2 T}{\partial x^2}+\frac{\partial^2 T}{\partial y^2}\right). \tag{4}$$

For convenience of numerical analysis, the following dimensionless parameters are introduced as

$$\eta=\frac{cx}{2\alpha},\quad \zeta=\frac{cy}{2\alpha},\quad \xi=\frac{t}{2\tau},\quad \theta=\frac{T-T_{in}}{T_0-T_{in}} \tag{5}$$

where T_{in} is the initial temperature, T_0 is the ambient temperature and c is the propagation speed of the thermal wave and is defined as $c=(\alpha/\tau)^{1/2}$. Thus the dimensionless form of equation (4) with these dimensionless variables in equation (5) can be written as

$$\frac{\partial^2\theta}{\partial\xi^2}+2\frac{\partial\theta}{\partial\xi}=\frac{\partial^2\theta}{\partial\eta^2}+\frac{\partial^2\theta}{\partial\zeta^2}. \tag{6}$$

In all illustrative examples of this paper, the initial conditions are given as

$$\theta(\eta,\zeta,0)=0$$

$$\frac{\partial\theta}{\partial\xi}(\eta,\zeta,0)=0.$$

Various types of the boundary conditions will be discussed in the following individual examples.

METHOD OF SOLUTION

To remove the ξ-derivative terms, the Laplace transform technique is employed. Taking the Laplace transform of equation (6) with respect to ξ gives

$$\frac{\partial^2\tilde{\theta}}{\partial\eta^2}+\frac{\partial^2\tilde{\theta}}{\partial\zeta^2}-(s^2+2s)\tilde{\theta}=0 \tag{7}$$

where s is the Laplace transform parameter and $\tilde{\theta}$ is the Laplace transform of the dimensionless temperature θ and is defined as

$$\tilde{\theta}(\eta,\zeta,s)=\int_0^\infty e^{-s\xi}\theta(\eta,\zeta,\xi)\,d\xi. \tag{8}$$

Subsequently, the control volume formulation is used

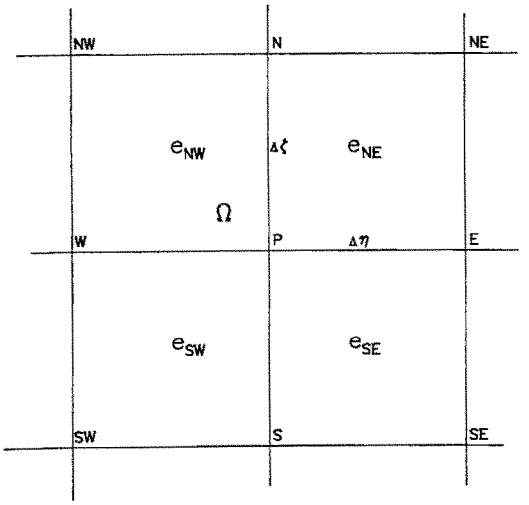

FIG. 1. Domain of Ω and four rectangular elements surrounding a typical interior point P.

to discretize equation (7). Integration of equation (7) within a control volume Ω gives

$$\int_{\Omega}\left[\frac{\partial^2\tilde{\theta}}{\partial\eta^2}+\frac{\partial^2\tilde{\theta}}{\partial\zeta^2}-(s^2+2s)\tilde{\theta}\right]d\eta\,d\zeta=0,\quad \eta,\zeta\in\Omega. \tag{9}$$

Before proceeding to discretize equation (9), we must approximate $\tilde{\theta}(\eta,\zeta,s)$ in terms of the nodal values and the shape functions within a typical element. For easy illustration, Fig. 1 shows the domain of interest Ω and four rectangular elements surrounding a typical interior point P in the (η,ζ) coordinate system. The domain of Ω in the present study is subdivided into a number of four-noded rectangular elements. First, the element e_{NE} with vertices P, E, NE and N is discussed, as shown in Fig. 1. The unknown function within e_{NE} $\tilde{\theta}(\eta,\zeta,s)$ can be approximated by

$$\tilde{\theta}(\eta,\zeta,s)=N_P(\eta,\zeta,s)\tilde{\theta}_P+N_E(\eta,\zeta,s)\tilde{\theta}_E+N_N(\eta,\zeta,s)\tilde{\theta}_N+N_{NE}(\eta,\zeta,s)\tilde{\theta}_{NE} \tag{10}$$

where these four nodal values are regarded as unknown at this stage, but are to be exactly specified later. N_P, N_E, N_N and N_{NE} are shape functions in the Laplce transform domain and are functions of the space variables. For the other three elements, $P-N-NW-W$, $P-S-SE-E$ and $P-W-SW-S$, $\tilde{\theta}$ can also be approximated in a similar way.

The shape functions can be chosen arbitrarily. However, as in the one-dimensional work considered earlier [15], the selection of the shape function in the transform domain is an important task for accurately predicting the propagation of the thermal wave. A poor selection of the shape functions will affect the stability of the numerical results. Tamma and Railkar [12] ever used the general solution of the transformed equation as the shape functions in their specially tailored transfinite-element formulations for one-dimensional hyperbolic heat conduction problems. However, it is sometimes difficult to find the general solution of a differential equation. Thus the technique in the authors' previous work [15] is extended to determine N_P, N_E, N_N and N_{NE}. The shape function $N_k(\eta,\zeta,s)$ is constructed such that it is unity at $\eta=\eta_k$ and $\zeta=\zeta_k$ and vanishes at the other three vertices of the same rectangular element. These four shape functions can be derived by using the following procedures.

The shape functions within the element e_{NE} are assumed to satisfy the homogeneous second-order partial differential equation

$$\frac{\partial^2 N_k}{\partial\eta^2}+\frac{\partial^2 N_k}{\partial\zeta^2}-\lambda^2 N_k=0,$$

$$\text{for } \eta_P\leqslant\eta\leqslant\eta_P+\Delta\eta,\quad \zeta_P\leqslant\zeta\leqslant\zeta_P+\Delta\zeta \tag{11}$$

where $\lambda^2=s^2+2s$.

By the separation of variables technique, $\tilde{\theta}$ can be expressed by

$$N_k(\eta,\zeta,s)=X(\eta,s)\cdot Y(\zeta,s). \tag{12}$$

Substituting equation (12) into equation (11) can yield

$$\frac{d^2X}{d\eta^2}-\mu^2X=0,\quad \text{for } \eta_P\leqslant\eta\leqslant\eta_P+\Delta\eta \tag{13a}$$

and

$$\frac{d^2Y}{d\zeta^2}-\mu^2Y=0,\quad \text{for } \zeta_P\leqslant\zeta\leqslant\zeta_P+\Delta\zeta \tag{13b}$$

where $\mu^2=\lambda^2/2$.

The approximation function of $N_k(\eta,\zeta,s)$ within the element e_{NE} can be written as

$$\begin{aligned}N_k=&A\cdot\sinh[\mu(1-\eta^*)\Delta\eta]\cdot\sinh[\mu(1-\zeta^*)\Delta\zeta]\\&+B\cdot\sinh[\mu\eta^*\Delta\eta]\cdot\sinh[\mu(1-\zeta^*)\Delta\zeta]\\&+C\cdot\sinh[\mu(1-\eta^*)\Delta\eta]\cdot\sinh(\mu\zeta^*\Delta\zeta)\\&+D\cdot\sinh(\mu\eta^*\Delta\eta)\cdot\sinh(\mu\zeta^*\Delta\zeta)\end{aligned} \tag{14}$$

where $\eta^*=(\eta-\eta_P)/\Delta\eta$ and $\zeta^*=(\zeta-\zeta_P)/\Delta\zeta$. A, B, C and D are determined from the constructed conditions of N_k. So, it is not difficult to derive these four shape functions N_P, N_E, N_N and N_{NE} as

$$N_P=\frac{1}{\sinh(\mu\Delta\eta)\cdot\sinh(\mu\Delta\zeta)}\sinh[\mu(1-\eta^*)\Delta\eta]\times\sinh[\mu(1-\zeta^*)\Delta\zeta] \tag{15a}$$

$$N_E=\frac{1}{\sinh(\mu\Delta\eta)\cdot\sinh(\mu\Delta\zeta)}\sinh(\mu\eta^*\Delta\eta)\times\sinh[\mu(1-\zeta^*)\Delta\zeta] \tag{15b}$$

$$N_N=\frac{1}{\sinh(\mu\Delta\eta)\cdot\sinh(\mu\Delta\zeta)}\sinh[\mu(1-\eta^*)\Delta\eta]\times\sinh(\mu\zeta^*\Delta\zeta) \tag{15c}$$

and

$$N_{NE} = \frac{1}{\sinh(\mu\Delta\eta)\cdot\sinh(\mu\Delta\zeta)}\sinh(\mu\eta^*\Delta\eta) \times \sinh(\mu\zeta^*\Delta\zeta). \quad (15d)$$

Similarly, the approximate function of N_k within the other three elements can be determined in the same way. It can be found that the bi-linear shape functions are the special case of the bi-hyperbolic shape functions. The hyperbolic function, $\sinh(z)$, can be expressed in a series form as

$$\sinh(z) = z + O(z^3). \quad (16)$$

With the error $O(z^3)$ for $\sinh(z)$, equations (15) are reduced to the following bi-linear shape function as

$$N_P = (1-\eta^*)\cdot(1-\zeta^*) \quad (17a)$$

$$N_E = \eta^*(1-\zeta^*) \quad (17b)$$

$$N_N = (1-\eta^*)\zeta^* \quad (17c)$$

and

$$N_{NE} = \eta^*\zeta^* \quad (17d)$$

where the bi-linear shape functions can be derived by taking the product of two one-dimensional linear shape functions. In other words, the shape functions for the two-dimensional element can be derived by processes identical to those described for one dimension.

It can be observed that node P is only associated with elements e_{NE}, e_{NW}, e_{SW} and e_{SE}. The discretized equation corresponding to node P will not be affected by the assembly of the contributions from the other elements. Thus the complete discretized equation for node P can be given by the assembly of the contributions from elements e_{NE}, e_{NW}, e_{SW} and e_{SE} as

$$a_P\cdot\tilde{\theta}_P + a_E\cdot\tilde{\theta}_E + a_W\cdot\tilde{\theta}_W + a_N\cdot\tilde{\theta}_N + a_S\cdot\tilde{\theta}_S + a_{NE}\cdot\tilde{\theta}_{NE} + a_{NW}\cdot\tilde{\theta}_{NW} + a_{SE}\cdot\tilde{\theta}_{SE} + a_{SW}\cdot\tilde{\theta}_{SW} = 0 \quad (18)$$

where

$$a_P = 4\left[\cosh(\mu\Delta\eta)\cosh\left(\mu\frac{\Delta\zeta}{2}\right) + \cosh(\mu\Delta\zeta)\cosh\left(\mu\frac{\Delta\eta}{2}\right) - \cosh(\mu\Delta\eta)\cosh(\mu\Delta\zeta)\right] \quad (19a)$$

$$a_E = a_W = 2\left[\cosh(\mu\Delta\zeta) - \cosh\left(\mu\frac{\Delta\zeta}{2}\right)\cosh(\mu\Delta\zeta)\right] \quad (19b)$$

$$a_N = a_S = 2\left[\cosh(\mu\Delta\eta) - \cosh\left(\mu\frac{\Delta\eta}{2}\right)\cosh\left(\mu\frac{\Delta\zeta}{2}\right)\right] \quad (19c)$$

and

$$a_{NE} = a_{NW} = a_{SE} = a_{SW} = \cosh\left(\mu\frac{\Delta\eta}{2}\right) + \cosh\left(\mu\frac{\Delta\zeta}{2}\right) - 2. \quad (19d)$$

The rearrangement of equations (19) with appropriate boundary conditions can yield the following vector–matrix equations as

$$[A]\{\tilde{\theta}\} = \{f\}. \quad (20)$$

The double-direct Guassian elimination algorithm and the numerical inversion of the Laplace transform proposed by Honig and Hirdes [16] is employed to invert the dimensionless temperature in the transform domain to the physical quantity. A two-dimensional computer code is written based on the above mathematical formulation. It is evident that two-dimensional HHC problems are much more difficult to solve than one-dimensional problems. The accuracy of this code will be evidenced against a two-dimensional HHC problem with analytical results.

ILLUSTRATIVE EXAMPLES

To demonstrate the successful application of the present numerical method to multidimensional HHC problems involving a case with the irregular geometry, three examples are illustrated below. The bi-linear shape functions can produce severe numerical oscillations in the vicinity of the thermal wave so that they will not be applied in the present study. All the computations are performed on a PC with an 80486 microprocessor and on the uniform space sizes $\Delta\eta = \Delta\zeta = 0.05$. It is obvious that the number of nodes required for the high-resolution numerical methods [14] is much larger than those required to model the present problem. Thus the cost and effort needed for Yang's solutions will be greater than those needed for the present solutions.

Example 1

To validate the accuracy of the present method, the first example concerned is a two-dimensional HHC in a semi-infinite strip, as shown in Fig. 2, with a constant thermal properties and with a uniform initial temperature $\theta = 0$. Suddenly, the wall at $\eta = 0$ is impulsively stepped to a temperature of the sine variation, i.e. $\theta(0, \zeta, \xi) = \sin(\pi\zeta)$. The boundary surfaces at $\zeta = 0$ and $\zeta = 1$ are kept at a constant temperature, $\theta = 0$. These boundary conditions are also shown in Fig. 2. The analytical solution of this problem can be easily obtained by using the Laplace transform method as

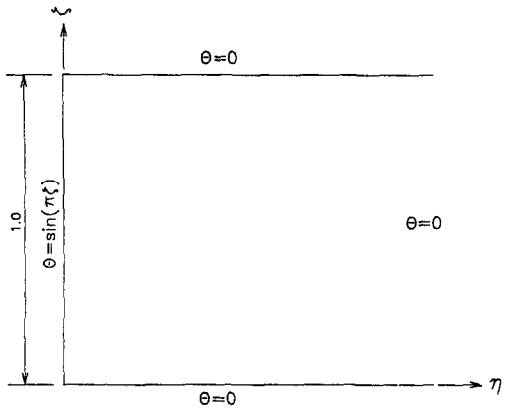

FIG. 2. Schematic diagram of Example 1.

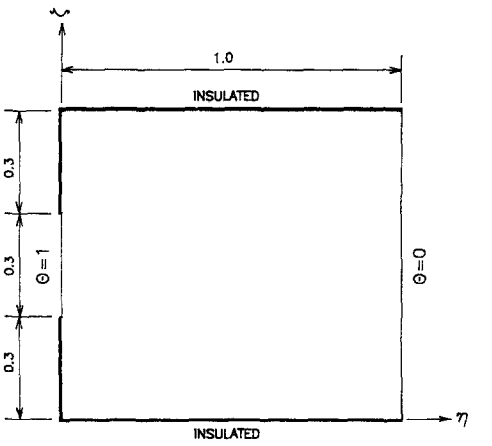

FIG. 3. Schematic diagram of Example 2.

$$\tilde{\theta}(\eta, \zeta, s) = \frac{1}{s} \cdot e^{-\eta(\lambda^2+\pi^2)^{1/2}} \cdot \sin(\pi\zeta). \quad (21)$$

Table 1 shows a comparison between the present results and the analytical solutions. It is seen that the present numerical solutions agree well with the analytical solution and do not exhibit severe numerical oscillations in the vicinity of the jump discontinuity. It is worth mentioning that the dimensionless temperature distribution at $\xi = \eta = 1$ has the jump discontinuity. This phenomenon is known as the Gibbs phenomenon, which is of practical importance since it is difficult to obtain a convergent solution in the neighbourhood of the jump discontinuity. The actual calculated values at points $(1, 0.25, 1)$ and $(1, 0.5, 1)$ are '0.1141' and '0.1614', respectively. In accordance with the Fourier convergence theorem [17], if the dimensionless temperature distribution at $\xi = \eta = 1$ and any ζ values has the jump discontinuity, the dimensionless temperature converges to the average value at the jump, namely, $\theta_c(1, \zeta, 1) = [\theta(1^-, \zeta, 1) + \theta(1^+, \zeta, 1)]/2.0$. Note that $\theta(1^+, \zeta, 1) = 0$ satisfies the problem boundary condition. Thus $\theta(1^-, \zeta, 1) = 2.0 \times \theta_c(1, \zeta, 1)$ is given in Table 1. This comparison implies that the present method has good accuracy for such problems. To further show the efficiency of the present method, the following examples will be illustrated.

Table 1. Comparison of the dimensionless temperature at $\xi = 1$

	$\zeta = 0.25$		$\zeta = 0.5$	
η	Present	Exact	Present	Exact
0	0.7071	0.7071	1.0	1.0
0.1	0.5141	0.5157	0.7271	0.7293
0.2	0.3748	0.3764	0.5301	0.5323
0.3	0.2756	0.2764	0.3897	0.3909
0.4	0.2053	0.2066	0.2903	0.2921
0.5	0.1602	0.1611	0.2265	0.2278
0.6	0.1358	0.1365	0.1920	0.1931
0.7	0.1312	0.1319	0.1855	0.1865
0.8	0.1471	0.1482	0.2081	0.2096
0.9	0.1882	0.1889	0.2661	0.2672
1.0	0.2282	0.2294	0.3228	0.3224
1.1	0.0	0.0	0.0	0.0
1.2		0.0	0.0	0.0

Example 2

The second illustrative problem concerns the propagation of the thermal wave in a rectangular cavity. The physical geometry of this problem is shown in Fig. 3. The cavity has a dimensionless length 1.0 and height 0.9. Initially, the slab is kept at a constant dimensionless temperature $\theta = 0$. For time $\xi > 0$, the heated region is centrally located at the left boundary surface and is one-third the size of the height. The temperature there is kept at a constant dimensionless temperature $\theta = 1$. The right boundary surface is kept at a constant dimensionless temperature $\theta = 0$. The rest of the boundary surfaces are insulated. Accordingly, the thermal waves will propagate towards the right and will expand into the top and bottom surfaces. Figures 4 and 5 show the propagations of the thermal wave in the cavity at various dimensionless times. Figure 4 shows the three-dimensional sketch of the dimensionless temperature at various dimensionless times. The phenomenon of the jump discontinuities, reflections and interactions can be obviously observed in Fig. 4. The isothermal distributions with a contour level of 0.05 at various dimensionless times are shown in Fig. 5. It is found from Fig. 5(b) that the thermal wave front reaches the top and bottom surfaces and is reflected at $\xi = 0.3$. Figure 5(c) shows that the thermal waves reflected from the top and bottom surfaces interact with the original thermal wave propagations at $\xi = 0.5$. At the dimensionless time $\xi = 1.0$, the thermal wave front reaches the right wall and is reflected. It can be noted from Figs. 4(e), 4(f), 5(e) and 5(f) that the strength of the original thermal discontinuity reduces with time due to heat diffusion. The temperature contours at $\xi = 5.0$ are essentially the same as those obtained from parabolic heat conduction. The multiple reflection feature of this problem shows a substantial difference between hyperbolic and parabolic heat conduction.

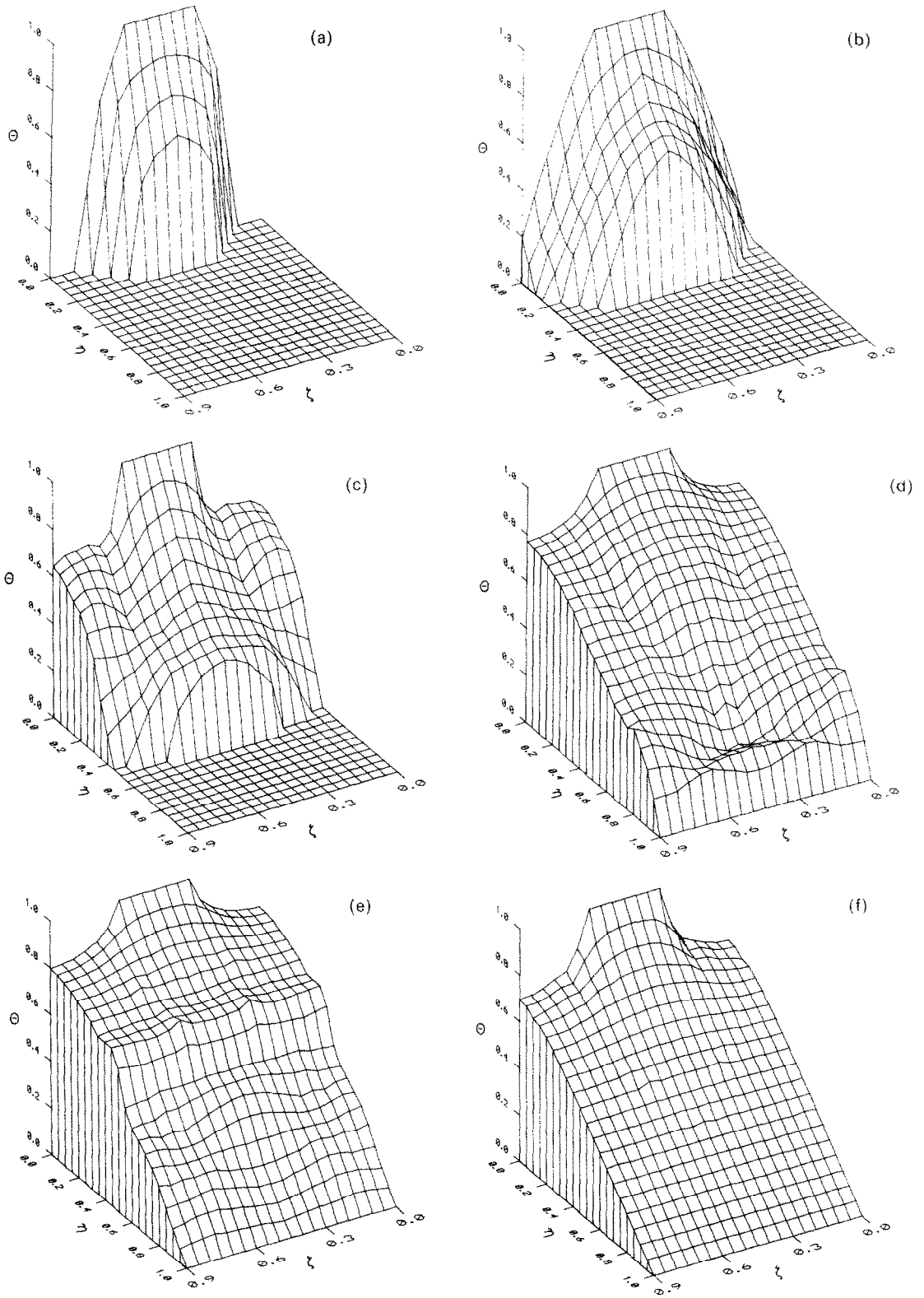

FIG. 4. Three dimensional sketch of the dimensionless temperature for Example 2 at various dimensionless times. (a) $\xi = 0.15$; (b) $\xi = 0.3$; (c) $\xi = 0.5$; (d) $\xi = 1.0$; (e) $\xi = 1.5$; (f) $\xi = 5.0$.

These phenomena agree well with those discussed in the work of Yang [14]. Moreover, the present results do not reveal severe numerical oscillations in the vicinity of the jump discontinuity. These results show that

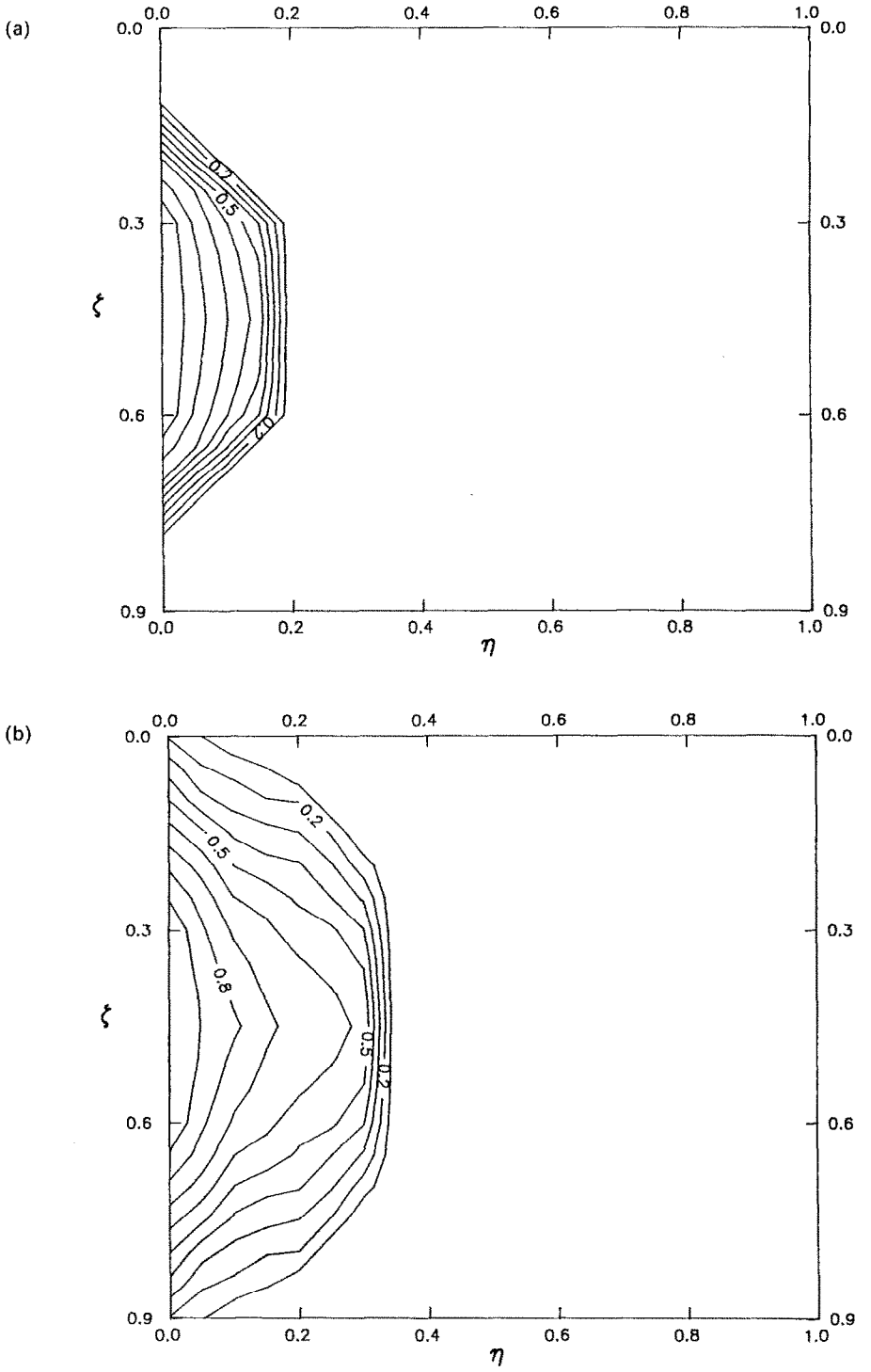

FIG. 5. Isothermal distributions with the contour level of 0.05 at various dimensionless times. (a) $\xi = 0.15$; (b) $\xi = 0.3$; (c) $\xi = 0.5$; (d) $\xi = 1.0$; (e) $\xi = 1.5$; (f) $\xi = 5.0$.

the present method can be successfully applied to analyze such problems.

Example 3

To show further the efficiency of the present method, this example studies the propagation of the thermal wave in an irregular geometry with a square attached to a semi-infinite strip, as shown in Fig. 6. The dimensionless length of the top and bottom walls in the left square is chosen as 0.3 and the height as 0.3. The dimensionless height of the right semi-infinite strip is chosen as 0.9. The boundary conditions are

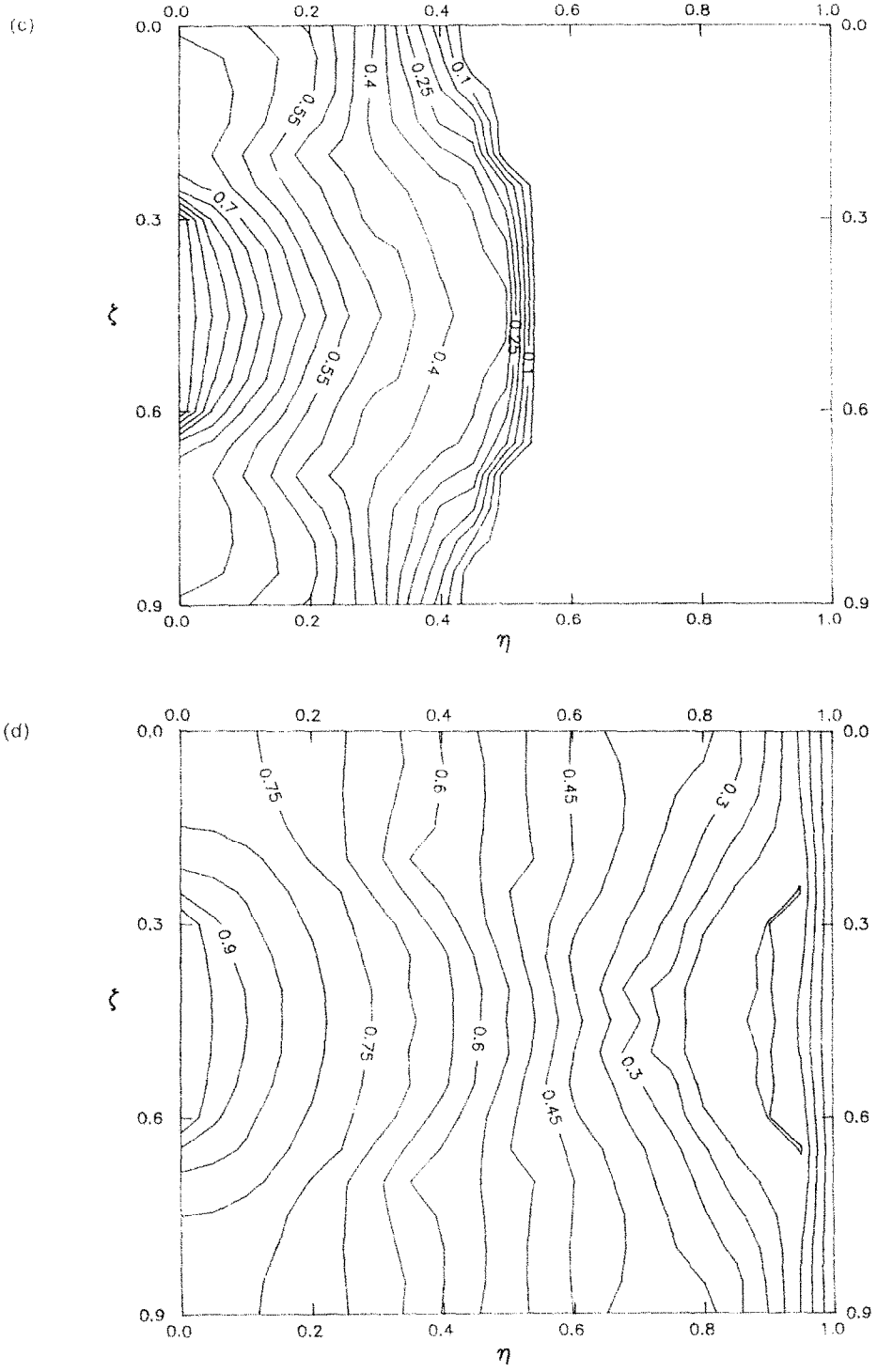

FIG. 5—*Continued.*

also shown in Fig. 6. Initially, this material is kept at a constant dimensionless temperature $\theta = 0$. For the dimensionless time $\xi > 0$, a constant heat flux is supplied on the left wall of the square. The heated region is centrally located at the left wall of the square. The dimensionless heat flux vector Q defined as $Q = (q/\rho C_p \alpha (T_0 - T_{in}))$ is introduced in the present problem. For convenience, Q is assumed to be unity in the present numerical computations.

The dimensionless form of equation (1) can be written as

$$\frac{\partial Q}{\partial \xi} + 2Q = -\frac{\partial \tilde{\theta}}{\partial \eta}\mathbf{i} - \frac{\partial \tilde{\theta}}{\partial \zeta}\mathbf{j}. \tag{22}$$

(e)

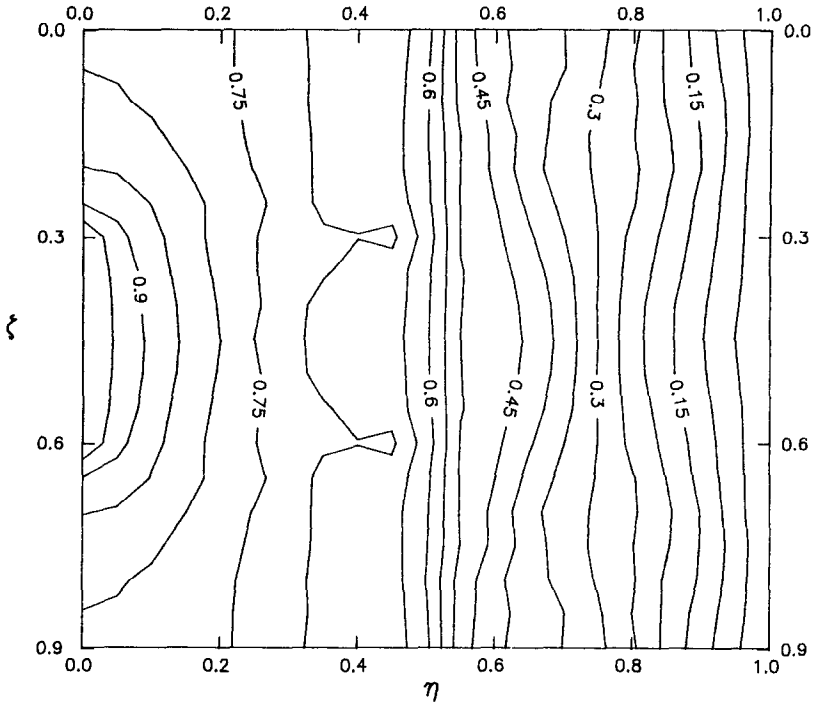

(f)

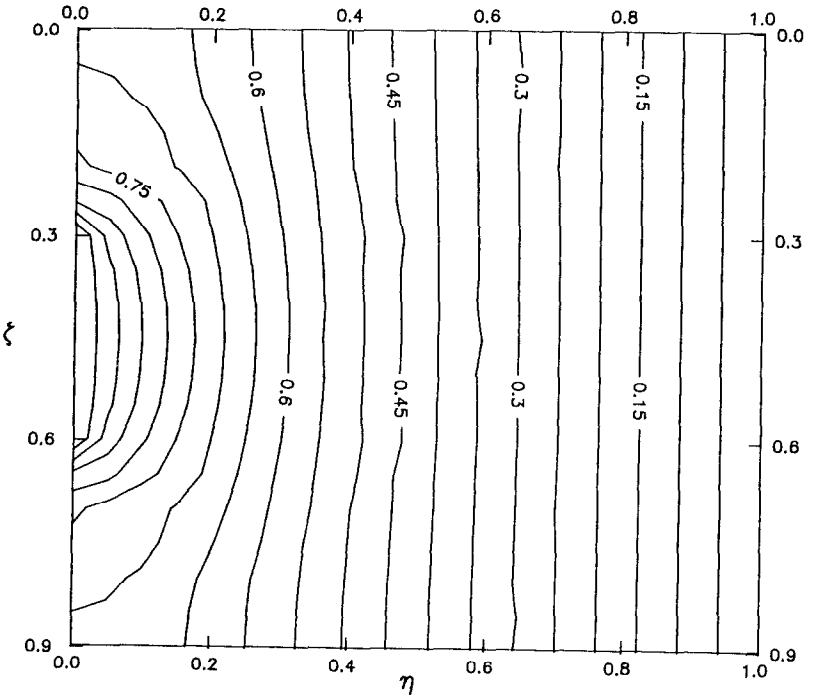

FIG. 5—*Continued.*

The Laplace transform of equation (22) is

$$(s+2)\cdot(\tilde{Q}_x\mathbf{i}+\tilde{Q}_y\mathbf{j}) = -\frac{\partial\tilde{\theta}}{\partial\eta}\mathbf{i}-\frac{\partial\tilde{\theta}}{\partial\zeta}\mathbf{j} \qquad (23)$$

where $\tilde{Q}_x$ and $\tilde{Q}_y$ are the components of the dimensionless heat flux vector in the η- and ζ-directions, and $\mathbf{i}$ and $\mathbf{j}$ denote the unit vectors in the η- and ζ-directions. The discretized equation for the left wall of the square subjected to the constant heat flux is given as

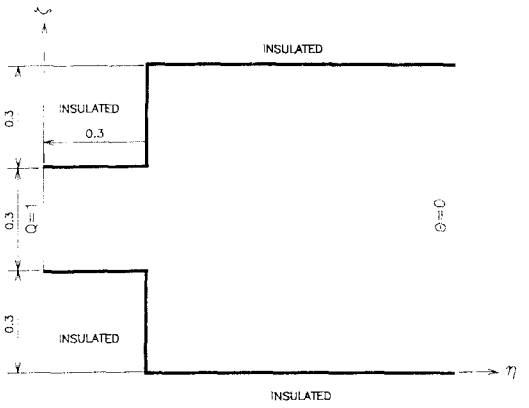

FIG. 6. Schematic diagram of Example 3.

$$a_P \cdot \tilde{\theta}_P + a_E \cdot \tilde{\theta}_E + a_N \cdot \tilde{\theta}_N + a_S \cdot \tilde{\theta}_S + a_{NE} \cdot \tilde{\theta}_{NE} + a_{SE} \cdot \tilde{\theta}_{SE} = f_P \quad (24)$$

where a_P, a_E, a_N, a_S, a_{NE} and a_{SE} have been given in equations (19). f_P is

$$f_P = -\sinh(\mu\Delta\eta)\sinh(\mu\Delta\zeta) \cdot (s+2) \cdot \tilde{Q}_c \cdot \Delta\zeta. \quad (25)$$

Due to the action of the dimensionless surface heat flux on the left wall of the square, the thermal waves will propagate towards the right and will expand into the top and bottom walls of the semi-infinite strip. The propagations of the thermal wave in the material at various dimensionless times are shown in Fig. 7. Figures 7(a) and (b) show that the propagations of

(a)

			0	0	0	0	0	0	0	0	0	0	0
			0	0	0	0	0	0	0	0	0	0	0
			0	0	0	0	0	0	0	0	0	0	0
1.14	.952	0	0	0	0	0	0	0	0	0	0	0	0
1.14	.952	0	0	0	0	0	0	0	0	0	0	0	0
1.14	.952	0	0	0	0	0	0	0	0	0	0	0	0
1.14	.952	0	0	0	0	0	0	0	0	0	0	0	0
			0	0	0	0	0	0	0	0	0	0	0
			0	0	0	0	0	0	0	0	0	0	0
			0	0	0	0	0	0	0	0	0	0	0

(b)

				0	0	0	0	0	0	0	0	0	0	0
				0	0	0	0	0	0	0	0	0	0	0
				0	0	0	0	0	0	0	0	0	0	0
1.28	1.09	.907	.368	0	0	0	0	0	0	0	0	0	0	0
1.28	1.09	.907	.368	0	0	0	0	0	0	0	0	0	0	0
1.28	1.09	.907	.368	0	0	0	0	0	0	0	0	0	0	0
1.28	1.09	.907	.368	0	0	0	0	0	0	0	0	0	0	0
				0	0	0	0	0	0	0	0	0	0	0
				0	0	0	0	0	0	0	0	0	0	0
				0	0	0	0	0	0	0	0	0	0	0

FIG. 7. Nodal temperature distributions of Example 3 at various dimensionless times. (a) $\xi = 0.15$; (b) $\xi = 0.3$; (c) $\xi = 0.6$; (d) $\xi = 1.2$.

(c)

			.533	0	0	0	0	0	0	0	0	0	0
			.719	.519	0	0	0	0	0	0	0	0	0
			.861	.673	.493	0	0	0	0	0	0	0	0
1.53	1.33	1.15	.963	.789	.619	.451	0	0	0	0	0	0	0
1.53	1.33	1.15	.978	.813	.654	.499	0	0	0	0	0	0	0
1.53	1.33	1.15	.978	.813	.654	.499	0	0	0	0	0	0	0
1.53	1.33	1.15	.963	.789	.619	.451	0	0	0	0	0	0	0
			.861	.673	.493	0	0	0	0	0	0	0	0
			.719	.519	0	0	0	0	0	0	0	0	0
			.533	0	0	0	0	0	0	0	0	0	0

(d)

			1.06	.934	.813	.709	.626	.559	.498	.453	0	0	0
			1.19	1.05	.912	.807	.723	.655	.587	.519	.275	0	0
			1.31	1.16	1.01	.904	.819	.734	.653	.472	.328	0	0
1.96	1.78	1.59	1.42	1.24	1.09	.984	.889	.801	.634	.491	.369	.268	0
1.99	1.76	1.58	1.44	1.31	1.19	1.05	.925	.774	.641	.519	.408	.309	0
1.99	1.76	1.58	1.44	1.31	1.19	1.05	.925	.774	.641	.519	.408	.309	0
1.96	1.78	1.59	1.42	1.24	1.09	.984	.889	.801	.634	.491	.369	.268	0
			1.31	1.16	1.01	.904	.819	.734	.653	.472	.328	0	0
			1.19	1.05	.912	.807	.723	.655	.587	.519	.275	0	0
			1.06	.934	.813	.709	.626	.559	.498	.453	0	0	0

FIG. 7—*Continued.*

the thermal wave at $\xi = 0.15$ and $\xi = 0.3$ look like those of one-dimensional thermal waves. It can be observed from Fig. 7(b) that the incident thermal shock has reached the right semi-infinite strip at $\xi = 0.3$. At $\xi = 0.6$, the thermal wave front reaches the top and bottom surfaces of the right semi-infinite strip, as shown in Fig. 7(c). However, in accordance with the variation of temperature shown in Fig. 7(d), the thermal waves have reflected from the top and bottom surfaces of the right semi-infinite strip interact with the propagation of the original thermal wave at $\xi = 1.2$.

CONCLUSIONS

The present study introduces an efficient numerical method to analyze two-dimensional HHC problems with irregular geometries. The major difficulty in the numerical analysis of HHC problems is the suppression of the numerical oscillations. As the thermal waves propagate with a finite speed, jump discontinuities will take place at the fronts of thermal wave propagations or interactions. As shown in the present results, the propagations, reflections and interactions of two-dimensional thermal waves are much more complicated than those of one-dimensional thermal waves. Thus multi-dimensional HHC problems are much more difficult to solve than one-dimensional problems. The present numerical scheme involving the hybrid applications of the Laplace transform technique and the control volume formulation is employed. The application of the Laplace transform technique can quickly give an accurate solution at a specific time without step-by-step computations in the time domain. This advantage can save the computing time and can avoid undesirable numerical oscillations due to a bad choice of time-step and space-step sizes. The key of the present numerical scheme is the selection of the shape functions used in the control volume formulation. Since the conventional bi-linear shape

functions will produce severe numerical oscillations in the numerical results, the bi-hyperbolic shape functions extended from the one-dimensional hyperbolic shape functions are used in the present study. It can be found from various illustrated results that the present numerical solutions do not reveal severe numerical oscillations in the vicinity of jump discontinuities. This conclusion implies that the bi-hyperbolic shape function shown in the present study can be a better choice for the present mathematical formulation. Moreover, the present method does not need to map the (x, y) coordinate system into the body-fitted coordinate system and to consider the effect of the CFL number on the numerical results.

REFERENCES

1. V. Peshkov, Second sound in helium II, *J. Phys. USSR* **8,** 381 (1944).
2. M. Human, Non-Fourier heat transfer in laser heated metal surfaces, *Heat Transfer: Korea–U.S.A. Seminar* (Edited by J. H. Kim *et al.*), pp. 521–533 (1986).
3. M. J. Maurer and H. A. Thompson, Non-Fourier effects at high heat flux, *J. Heat Transfer* **95,** 284–286 (1973).
4. C. Cattaneo, On the conduction of heat, Atti Del Seminar, Mat. Fis. Univ., *Modena* **3,** 3 (1948).
5. M. P. Vernotte, Les paradoxes de la theorie continue de l'equation de la chaleur, *Comptes Rendus Acad. Sci.* **246,** 3154–3155 (1958).
6. S. Sieniutycz, The variational principle of classical type for non-coupled non-stationary irreversible transport processes with convective motion and relaxation, *Int. J. Heat Mass Transfer* **20,** 1221–1231 (1977).
7. A. V. Luikov, Application of irreversible thermodynamics methods to investigation of heat and mass transfer, *Int. J. Heat Mass Transfer* **9,** 139–152 (1966).
8. W. Kaminski, Hyperbolic heat conduction equation for materials with a nonhomogeneous inner structure, *J. Heat Transfer* **112,** 555–560 (1990).
9. K. J. Baumeister and T. D. Hamill, Hyperbolic heat-conduction equation—a solution for the semi-infinite body problem, *J. Heat Transfer* **91,** 543–548 (1969).
10. G. F. Carey and M. Tsai, Hyperbolic heat transfer with reflection, *Numer. Heat Transfer* **5,** 309–327 (1982).
11. D. E. Glass, M. N. Özisik, D. S. McRae and B. Vick, On the numerical solution of hyperbolic heat conduction, *Numer. Heat Transfer* **8,** 497–504 (1985).
12. K. K. Tamma and S. B. Railkar, Specially tailored transfinite-element formulations for hyperbolic heat conduction involving non-Fourier effects, *Numer. Heat Transfer* **B15,** 211–226 (1989).
13. H. Q. Yang, Characteristics-based, high-order accurate and nonoscillatory numerical method for hyperbolic heat conduction, *Numer. Heat Transfer* **B18,** 221–241 (1990).
14. H. Q. Yang, Solution of two-dimensional hyperbolic heat conduction by high-resolution numerical methods, *Numer. Heat Transfer* **A21,** 333–349 (1992).
15. H. T. Chen and J. Y. Lin, Numerical analysis for hyperbolic heat conduction, *Int. J. Heat Mass Transfer* **36,** 2891–2898 (1993).
16. G. Honig and U. Hirdes, A method for the numerical inversion of Laplace transforms, *J. Comput. Appl. Math.* **10,** 113–132 (1984).
17. M. D. Greenberg, *Advances Engineering Mathematics*, pp. 461–465. Prentice-Hall, New Jersey (1988).